A Non-dimensional Characterization of Structural Vibration Induced Vertical Slosh Damping

Michael Wright
Industrial CFD Research Group, Department of Mechanical Engineering, University of Cape Town,
Cape Town, South Africa. (http://www.incfd.uct.ac.za/)

Francesco Gambioli
Technical Skill Leader - Wing, Loads and Aeroelastics Department, Airbus,
Filton, England, United Kingdom
Dept. of Mechanical and Aerospace Engineering, Sapienza University of Rome,
Rome, Italy

Arnaud G. Malan
Professor and South African Research Chair in Industrial CFD, Industrial CFD Research Group,
Department of Mechanical Engineering, University of Cape Town, Cape Town, South Africa. (http://www.incfd.uct.ac.za/)

ABSTRACT

This paper aims to present a non-dimensional analysis which characterises the structural vibration induced slosh damping for a single-degree-of-freedom (SDOF) tank system under vertical motion. We identify several key non-dimensional relations which are then characterised in terms of slosh loads and dissipated power using volume of fluid (VoF) computational fluid dynamics (CFD) simulations. Scaling-laws are then constructed for future quantification of these phenomena. The fitted scaling rules are shown to offer a clear correlation for the selected SDOF system, contingent on minimal changes to the flow Weber number.

KEY WORDS: Sloshing; Non-dimensional Analysis; CFD; Damping

INTRODUCTION

The modelling of liquid-gas free-surface interaction (sloshing) within tanks and containers is an area of interest within the aerospace industry, impacting the aerodynamic stability and aircraft control characteristics during flight, ground manoeuvres and loads. As such the EU H2020 SLOWD (SLOshing Wing Dynamics) (Gambioli et al. 2020) aims to characterise and model the impact of fuel sloshing on the damping characteristics of a wing structure due to vertical excitation where the direction of excitation is normal to the liquid free-surface. The preceding Protospace tests (Titurus et al. 2019, Gambioli et al. 2019) proved that fuel sloshing provides significant damping to a cantilever based fuel tank undergoing free-vibration due to an initial structural perturbation. In this case, the fundamental frequency of excitation was found to remain constant. This article, therefore, focuses on non-dimensionally characterising the liquid slosh induced damping due to a fixed frequency damped vibration ω. The structure (in this case a cantilever beam) is equivalent in dynamics to a mass-spring-damper system which is excited via an initial displacement.

Due to the laboratory scale of the cited experiments (Gambioli et al. 2019, Titurus et al. 2019), increased understanding of the bias introduced by geometric scaling is a key objective of the SLOWD project. This will further enable the development of suitable similarity parameters and isolate the effects introduced by non-ideal (practical) scaling in assessing the influence of sloshing on the structural dynamics of aircraft wings. Once validated, the use of CFD has proven crucial in such studies, as it allows for the study of a wide range of parameters and their combinations, which are impractical with real-fluids.

It is widely accepted that non-dimensional analysis provides a powerful analytical technique to characterise a complex physical system. This enables the study and quantification of the relative importance of various physical parameters/phenomena on such systems (Gibbings 2011). Despite the insights that non-dimensional analyses provide, limited studies of violent slosh through such techniques exist in literature. Thompson & Nein (1966) successfully employed dimensional analysis as a method to predict the pressurisation requirements for space vehicles at launch and a generalisation of slosh force subject to several excitation frequency parameters for various tank geometries (Summer 1963).

Past work into the application and tuning of liquid damping systems has centred on structural design and civil engineering applications (Yu et al. 1999, Tait 2008). Previous aeroelastic studies into the influence of slosh damping within the aerospace field focus on the general trends and

changes in flutter boundaries due to various tank fill-level configurations (Konopka et al. 2019). These campaigns neglected vertical motion of the tank, employing seismic shaking tables to provide the excitation to the structure.

This paper proposes a non-dimensional analysis for an SDOF tank system to identify fluid specific non-dimensional relationships to characterise slosh damping due to vertical structurally induced excitation. Furthermore, to employ the rigorously validated VoF CFD code ELEMENTAL® (Pattinson et al. 2007, Malan & Oxtoby 2013, Heyns et al. 2013*b*,*a*, Oxtoby et al. 2015, Jones et al. 2019, Ilangakoon et al. 2020) to quantify the scaling of slosh physics such as kinetic energy, slosh loads and dissipated power, as a function of selected non-dimensional numbers. Such scaling studies are impossible to conduct via laboratory size experimental campaigns due to limitations in fluid availability.

To this end, we employ a single compartment of the Protospace experimental tank (Gambioli et al. 2019) with a 50% fill-level undergoing a damped sinusoidal vertical excitation. In this work, it is simulated using a two-dimensional rectangular tank with a height of $0.06m$ and width of $0.11m$. Having been validated previously against the measured data, the 2D CFD then enables the modification of various fluid properties and excitation frequencies to complete the analysis.

This paper is organised as follows:

1 We present of a non-dimensional analysis of an SDOF tank under vertical slosh, isolating the functional relationship characterising slosh damping.

2 We define the non-dimensional parameter space of interest for the problem under consideration.

3 We describe the analysis of system-fluid energies, slosh loads and power due to the scaling of selected non-dimensional numbers.

4 Finally, we identify scaling-laws for the dissipated power due to the previous scaling by means of curve fitting of CFD results, these are evaluated against selected high-fidelity VoF test cases.

DIMENSIONAL ANALYSIS

Table 1 Dimensional Matrix

Quantity			*Units*		
			M	L	T
μ	Liquid Viscosity	$[Pa.s]$	1	-1	-1
ρ	Liquid Density	$[kg.m^{-3}]$	1	-3	0
ρ_{air}	Gas Density	$[kg.m^{-3}]$	1	-3	0
γ	Liquid Surface Tension	$[N.m^{-1}]$	1	0	-2
θ	Liquid-Solid Contact Angle	$[rad]$	0	0	0
v	Liquid Velocity	$[m.s^{-1}]$	0	1	-1
g	Gravity	$[m.s^{-2}]$	0	1	-2
m	Solid Mass	$[m]$	1	0	0
k	Structural Stiffness	$[N.m^{-1}]$	1	0	-2
c	Structural Damping	$[Ns.m^{-1}]$	1	0	-1
h	Tank Height	$[m]$	0	1	0
l	Tank Length	$[m]$	0	1	0
η_0	Height of fluid	$[m]$	0	1	0
y_0	Initial tank offset (spring displacement)	$[m]$	0	1	0

In an attempt to limit the scope of this paper, the non-dimensional analysis is done using standard atmospheric conditions. As such, all simulations employ air at STP as the gas within the liquid-gas slosh system. This restriction enables the limitation of the number of parameters considered in the non-dimensional study. Therefore the 14 parameters considered relevant for the vertical oscillation of a rectangular 2D tank supported by a mass-spring-damper system are presented with Table 1. Also included are entries of the dimensional matrix for the units of Mass (M), Length (L) and Time (T).

The rank 3 dimensional matrix employs the normalisation of length (h), mass (ρh^3) and time ($\frac{1}{\omega}$) respectively. A straightforward application of the Buckingham Pi Theorem leads to $14 - 3 = 11$ dimensionless groups:

$$\begin{aligned}
&\pi_1 = \frac{m}{\rho h^3} = \bar{m} && \pi_2 = \frac{\rho_{Air}}{\rho} = \bar{\rho} && \pi_3 = \frac{\rho v h}{\mu} = Re_v \\
&\pi_4 = \frac{v}{\sqrt{gh}} = Fr_v && \pi_5 = \frac{\rho v^2 h}{\gamma} = We_v && \pi_6 = \frac{k}{\rho h^3}\frac{h}{v} \\
&\pi_7 = \frac{c}{\rho h^3}\frac{h}{v} && \pi_8 = \theta && \pi_9 = \frac{l}{h} = \tilde{A} \\
&\pi_{10} = \frac{\eta_0}{h} = \tilde{F} && \pi_{11} = \frac{y_0}{h} = \tilde{Y}_0 &&
\end{aligned} \tag{1}$$

We define the first groups π_1 and π_2 as the solid to liquid mass ratio $\bar{m}$ of the one-degree of freedom system and density ratio $\bar{\rho}$ of the gas and liquid phase in the tank. π groups 3 to 5 are well known dimensionless numbers, namely the Reynolds, Froude and Weber. Note that in this work we define We_v as the standard definition based on the fluid velocity. Considering damped harmonic motion at frequency ω enables the derivation of the reference velocity in terms of the slosh-mass-spring-damper system response as:

$$v = \omega h \tag{2}$$

We can therefore modify π groups 3 to 5 as follows

$$\pi_3' = \frac{\rho\omega h^2}{\mu} = Re \qquad \pi_4' = \omega\sqrt{\frac{h}{g}} = Fr \qquad \pi_5' = \frac{\rho\omega^2 h^3}{\gamma} = We \tag{3}$$

where Re, Fr and We are the excitation frequency based Reynolds, Froude and Weber numbers respectively. The Froude number as a function of the frequency parameter therefore infers a reduced frequency or a Strouhal number. Thus representing the ratio of the characteristic time of the mechanical system and the fluid-characteristic time. Finally, the manipulation of π_6 and π_7 by combining with π_1 provides:

$$\pi_6' = \sqrt{\frac{\pi_6}{\pi_1}} = \sqrt{\frac{k}{m}}\frac{h}{v} = \frac{\omega}{\omega} = 1 \qquad \pi_7' = \frac{\pi_7}{2\pi_1} = \frac{c}{2m\omega} = \xi \tag{4}$$

For π_7 we employ the standard definitions of the natural frequency of excitation ω and the structural damping ratio ξ for harmonic oscillators $\omega = \sqrt{\frac{k}{m}}$ and $\xi = \frac{c}{2m\omega}$. The result of π_6 is a direct consequence of choosing $1/\omega$ as a time parameter. Here ξ denotes the total damping of the system.

To justify the choice of h as the characteristic length π_9, π_{10} and π_{11} are derived by dividing all other relevant geometrical quantities by the characteristic length. Here $\tilde{A}$ is the tank aspect ratio, $\tilde{F}$ the liquid fill ratio and $\tilde{Y}_0$ the dimensionless initial deflection of the mass-spring system. For the slosh case considered in this article, these quantities are $O(1)$ and as a result the liquid centre of gravity displacements and wave height. The latter is a consequence of the slosh being within the physical bounds of the tank. Therefore, the derivation of a functional relationship to characterise the fluid-structure-system-damping will employ the remaining π groups:

$$\xi = f\left(\bar{m}, \bar{\rho}, Re, Fr, We, \theta, \tilde{A}, \tilde{F}, \tilde{Y}_0\right) \tag{5}$$

The intention to investigate the slosh damping through comparative studies requires the decomposition of the total system damping into its components. This decomposition enables the isolation of the slosh damping as a function of the total-damping measured and damping measured for solid (dry) mass simulations, such that:

$$\xi = \xi_d + \Delta\xi_s \tag{6}$$

where ξ, ξ_d and $\Delta\xi_s$ are the total system damping, structural (dry) damping ratio and slosh damping respectively. Therefore the derivation of a functional relationship characterising the slosh damping results in the form:

$$\Delta\xi_s = F\left(\bar{m}, \bar{\rho}, Re, Fr, We, \theta, \tilde{A}, \tilde{F}, \tilde{Y}_0, \xi_d\right) \tag{7}$$

From the above, we can identify three distinct groups of dimensionless numbers influencing the slosh damping within the SDOF system. The three groups are sloshing flow (fluid specific non-dimensional numbers such as $\bar{\rho}$, Re, Fr, We and θ), fluid-structure interactions and geometric non-dimensional factors. This paper employs high fidelity VoF CFD to investigate the influence of the sloshing flow parameters. The use of validated CFD for this purpose enables the scaling of various fluid properties as listed in Table 3, and such that only a single non-dimensional number is effected. This would be impractical/impossible via experimental means.

To investigate the influence of the selected non-dimensional properties on the slosh damping requires measuring the damping response for a fully coupled fluid-structure interaction (FSI) simulation. Alternatively, the trends on the system damping for the non-dimensional scaling can be related to the average dissipated power due to the dry damping force on the system (P_{Disp}) using the definition of the dissipated power per cycle in a mechanical oscillator as (van Biezen 2014)

$$P_{Disp} \propto \xi m\omega^3 y_0^2 \;\rightarrow\; \xi \propto \frac{P_{Disp}}{m\omega^3 y_0^2} \tag{8}$$

where,

$$P_{Disp} = \frac{\int_0^t \boldsymbol{F}\cdot\boldsymbol{v}dt}{t} \tag{9}$$

The above relation is due to observations made during the initial Protospace experiment. Here, the global motion of the liquid centre of mass is of the same order as that of the overall tank (which is the case for the problem under consideration). Therefore the damping ratio ξ is directly proportional to the dissipated power. This relationship enables the use of forced harmonic excitations of the fluid volume only (as opposed to an FSI simulation) to quantify the slosh damping due to the scaling of selected non-dimensional properties.

NON-DIMENSIONAL PROPERTY PARAMETER SPACE

The initial Protospace experiment (Gambioli et al. 2019) aimed to provide a Froude scaled aircraft wing with a geometry scaling of $\lambda = 0.2$ while employing water whereas the full-scale model makes use of cold kerosene. The calculation of non-dimensional values for both the Protospace, full-scale model and the ratio between the two experiments, are given in Table 2. Accordingly, the range of the non-dimensional parameter space was chosen to contain both the Protospace and full-sized model non-dimensional values, as presented in Table 3.

Table 2 Protospace vs Full Aircraft Non-dimensional Properties

Non-Dimensional Quantity	*Protospace*	*Aircraft*	*Ratio*
$\bar{\rho}$	1.23×10^{-3}	1.64×10^{-3}	1.33
Re	161.58×10^3	45.12×10^3	0.279
Fr	3.440	3.440	1
We	5785.917	79.71×10^3	13.78

Table 3 Non-dimensional property parameter space

Parameter		*Property Range*
θ	$\in [0.524, 1.506]$	–
$\bar{\rho}$	$\in [6.494 \times 10^{-4}, 6.181 \times 10^{-3}]$	$\therefore \rho \in [199, 1894]$
Re	$\in [42.56 \times 10^3, \infty)$	$\therefore \mu \in [0, 3.7 \times 10^{-3}]$
We	$\in [4.92 \times 10^3, 1.37 \times 10^5]$	$\therefore \gamma \in [0.003, 0.0847]$
Fr	$\in [0.688, 6.879]$	$\therefore f \in [1.4, 14]$

The CFD simulations to follow employ a single compartment tank undergoing a damped sinusoidal vertical acceleration defined by,

$$a(t) = -a_0\, e^{-\zeta 2\pi f t}\, cos(2\pi f t) \tag{10}$$

where $a_0 = 200m.s^{-2}$ and $\zeta = 0.06$ (measured from the Protospace experiment). The computed energy budget, slosh loads and time are normalised to the potential energy change (E_u) of the system, the frozen mass model and by the excitation frequency respectively. The normalised forms of the ~~fluid~~ dissipation energy (E_{Diss}), surface work (W_s), vertical sloshing force (F_y) and oscillation count ($n_{oscillation}$) are defined such that,

$$\begin{aligned} ||E_{Diss}|| &= \frac{E_{Diss}}{E_u} & ||W_s|| &= \frac{W_s}{E_u} \\ ||F_y|| &= \frac{F_y}{max(|F_y|)} & n_{oscillation} &= \frac{t}{\omega} \end{aligned} \tag{11}$$

This normalisation enables the direct comparison of simulations with differing excitation frequency and liquid masses.

RESULTS AND ANALYSIS

Fluid Properties Scaling

Fig. 1 presents comparative ranges for the influence on the normalised sloshing fluid dissipation energy ($||E_{Diss}||$), surface work ($||W_s||$) and vertical sloshing force ($||F_y||$). The influence range of each non-dimensional number on the selected quantities are presented by means of a shaded region.

Table 4 RMSE Variation due to the Fluid Property Scaling of Protospace (%)

	$\|\|E_{Diss}\|\|$	$\|\|W_s\|\|$	$\|\|F_y\|\|$
Re	6.844	3.610	11.897
$\bar{\rho}$	5.956	3.162	10.489
We	8.561	4.938	1.727
θ	6.169	3.338	.164
$\theta = 90°$	99.179	45.808	38.705

The percentage variation for each simulation against said Protospace benchmark ~~is calculated for each property against~~ the maximum value of the property from ~~said~~ Protospace benchmark. These quantities enable the calculation of a root-mean-square error (RMSE) of the influence of each scaled property to be evaluated and compared, ~~as presented in Table 4.~~ The analysis reveals the relatively low ~~impact of scaling the~~

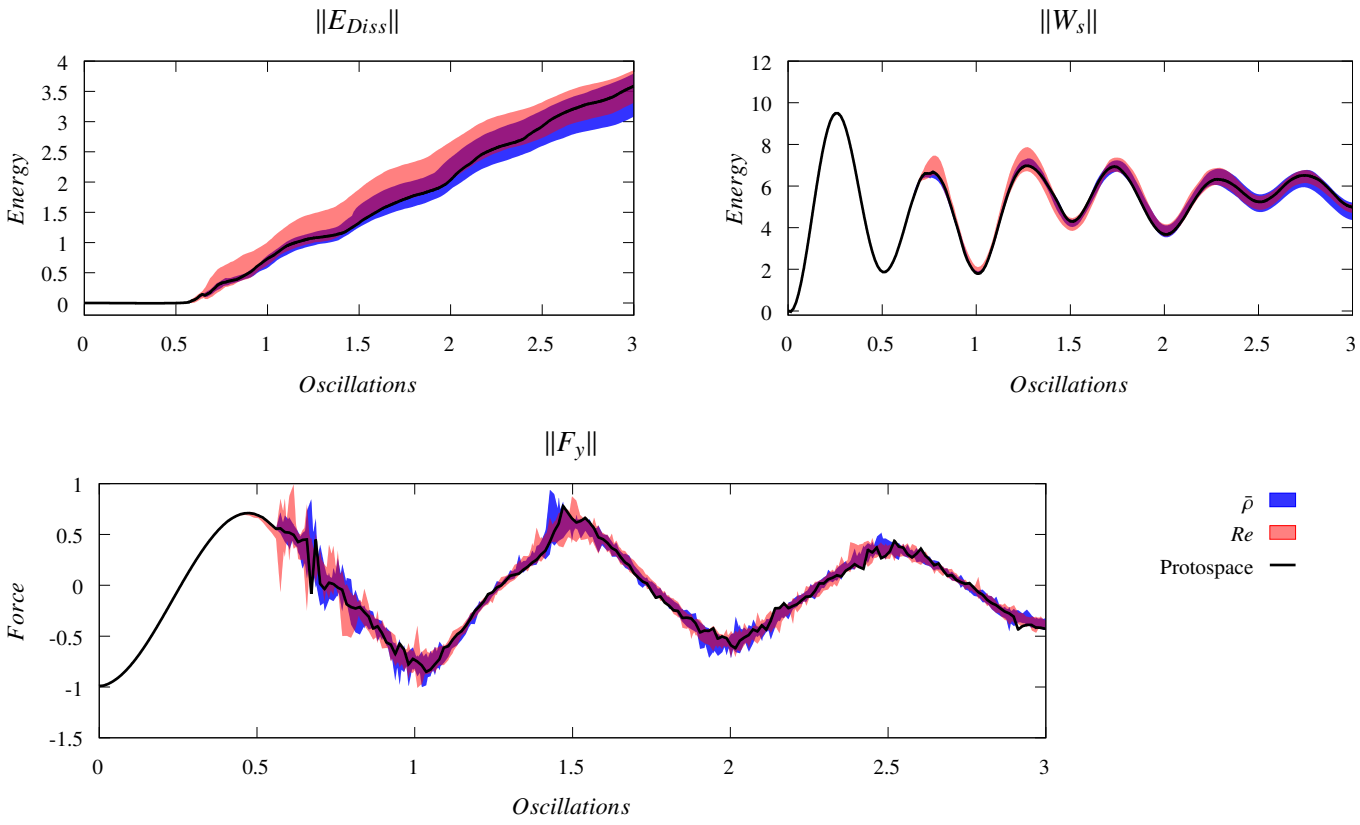

(a) Density Ratio and Reynolds Number Scaling

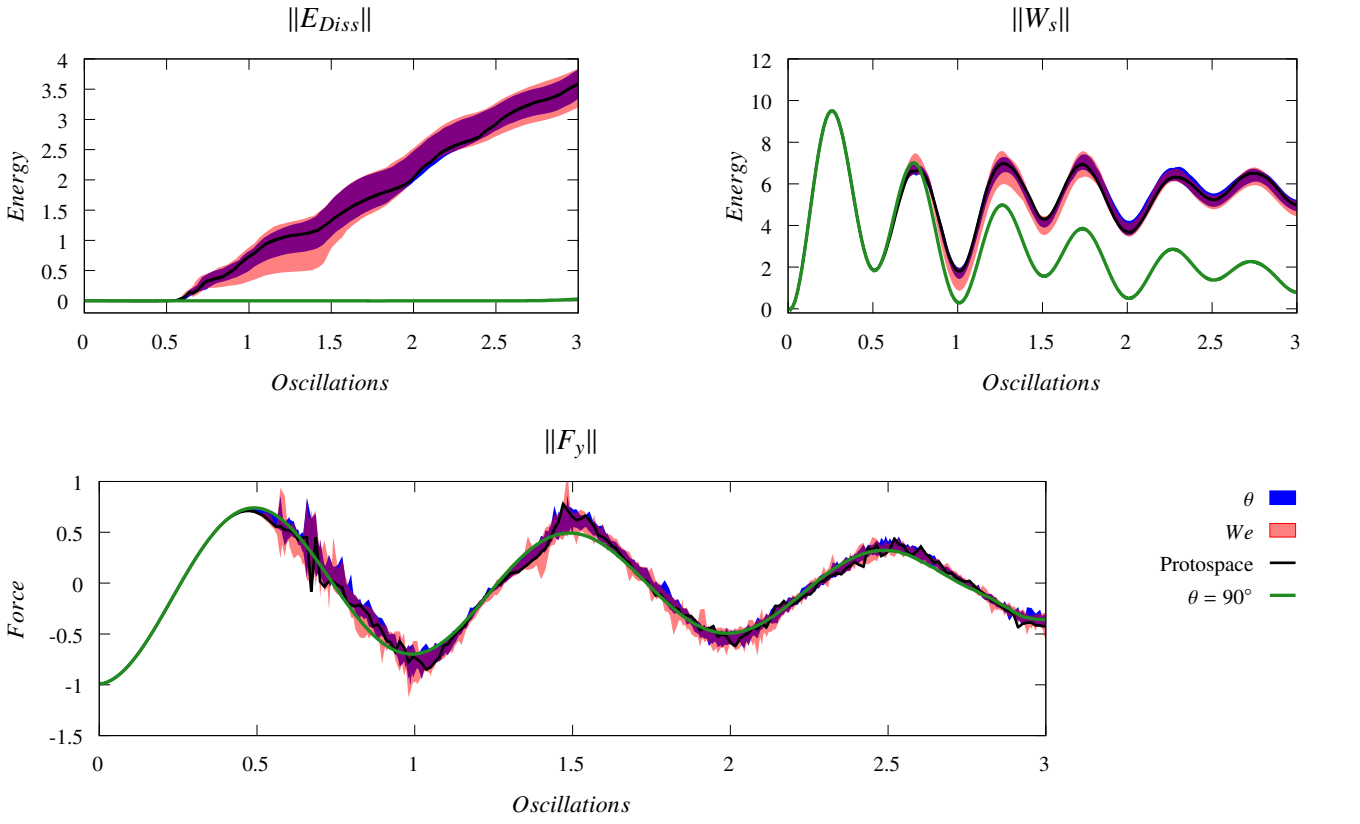

(b) Fluid Surface Tension Properties

Fig. 1 Influence of Fluid Properties on Selected Normalised System Energies and Slosh Loads

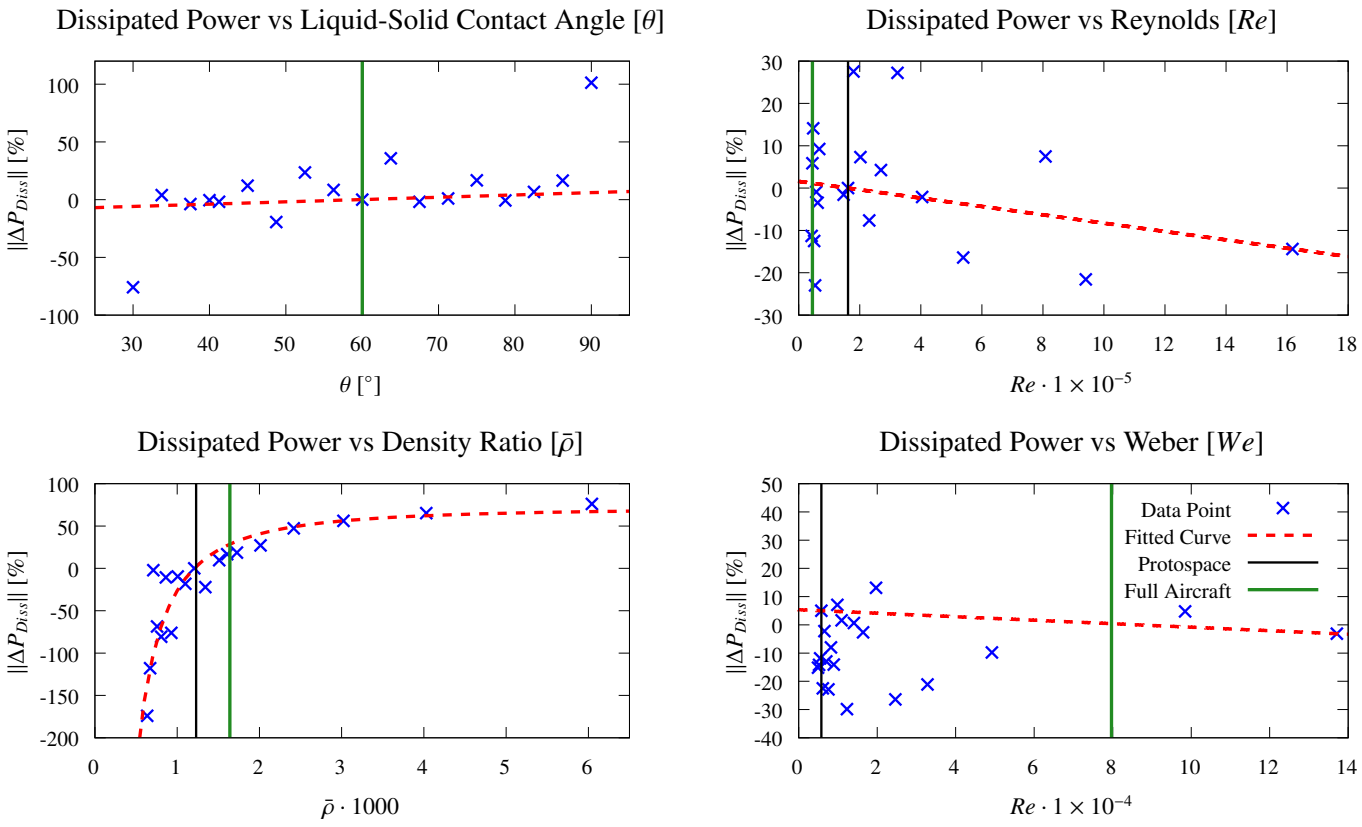

Fig. 2 Dissipated Power due to various Fluid Properties

fluid properties on ~~the~~ $\|E_{Diss}\|$ where the RMSE < 10% and negligible on $\|W_s\|$ as RMSE < 5%.

~~The scaling of fluid properties is shown to have a moderate influence on the slosh loads (F_y) when compared against the Protospace benchmark where the RMSE < 12%. The maximum RSME impact on the slosh loads occurs due to the scaling of Re followed by We, $\bar{\rho}$ and θ.~~

The prescription of a damped harmonic motion within the simulation results in two dissipative forces, namely the dry damping force (due to the prescribed damped motion) and the forces exchanged between the tank and the mass-spring-damper system (slosh loads). Therefore the average dissipative power (P_{Disp}) due to slosh loads on the SDOF can be calculated as,

$$P_{Disp} = \frac{\int_0^t F_y v_y dt}{t} \tag{12}$$

The ~~calculation of a percentage scaling factor~~ ($\|\Delta P_{Disp}\|$) ~~between P_{Disp}(Protospace) and a selected non-dimensional scaled simulation such that,~~

$$\|\Delta P_{Disp}\| = \frac{P_{Disp} - P_{Disp}(\text{Protospace})}{|P_{Disp}(\text{Protospace})|} \tag{13}$$

Plotting ~~the~~ $\|\Delta P_{Disp}\|$ against the scaled values of the properties allows for the identification of scaling-laws. Fig. 2 presents the discrete $\|\Delta P_{Disp}\|$ values for individually scaled non-dimensional numbers and the general trend established for the discrete points. ~~These general trends provide scaling-laws and a method to estimate the scaling effects of specific fluid properties for the selected system.~~

While no significant statistical trend for $\|\Delta P_{Disp}\|$ exists for the scaling of We and Re, the fitting of a general linear trend for the scaling of θ highlights the low impact to $\|\Delta P_{Disp}\|$ across the majority of the parameter space. Outliers to this trend occur due to the Rayleigh Taylor instability where $\theta = 90°$ which leads to $P_{Disp} \to 0$ and an ~~artificially~~ enlarged meniscus as $\theta \to 0$ ~~resulting in the dominate reaction of the sloshing system being due to the meniscus collapse as opposed to the vertical excitation.~~

$$\|\Delta P_{Disp}(\bar{\rho})\| = -1.11 \times 10^{-3}\bar{\rho}^{-1.65} + 72.05 \qquad r^2 = 0.934 \tag{14}$$

A well defined trend can be fitted for the scaling of $\bar{\rho}$ as described by Eq. 14 provides ~~a high accurate fit to the s results whereas $\bar{\rho} \to 0$, $\|\Delta P_{Disp}\| \to \infty$ and as $\bar{\rho} \to \infty$, $\|\Delta P_{Disp}\| \to \approx 70\%$.~~ The asymptotic behaviour of the fitted curve provides a minimum P_{Disp} due to a two fluid system undergoing the given excitation with STP water θ and a constant Re and We value, these constants may be responsible for the asymptotic behaviour where at low fluid densities these properties govern the dissipative power.

~~Presenting the analysis for the case where $\theta = 90°$ shows the dominant influence of Rayleigh Taylor instabilities on the system energies and loads viz. the variance on $\|E_{Diss}\| = 99.179\%$, $\|W_s\| = 45.808\%$ and $\|F_y\| = 38.705\%$. The absence of surface instability results in negligible dissipated power whereby $P_{Disp}(\theta = 90°) = 0.17W$ when compared to the Protospace simulation P_{Disp}(Protospace) $= -13.91W$.~~

Simulation Property Scaling

Fig. 3 presents the influence range of the scaling of ~~Fr~~. A similar statistical analysis as performed to create Table 4 is employed to provide Table 5. The increased sensitivity of the systems energy balance to the

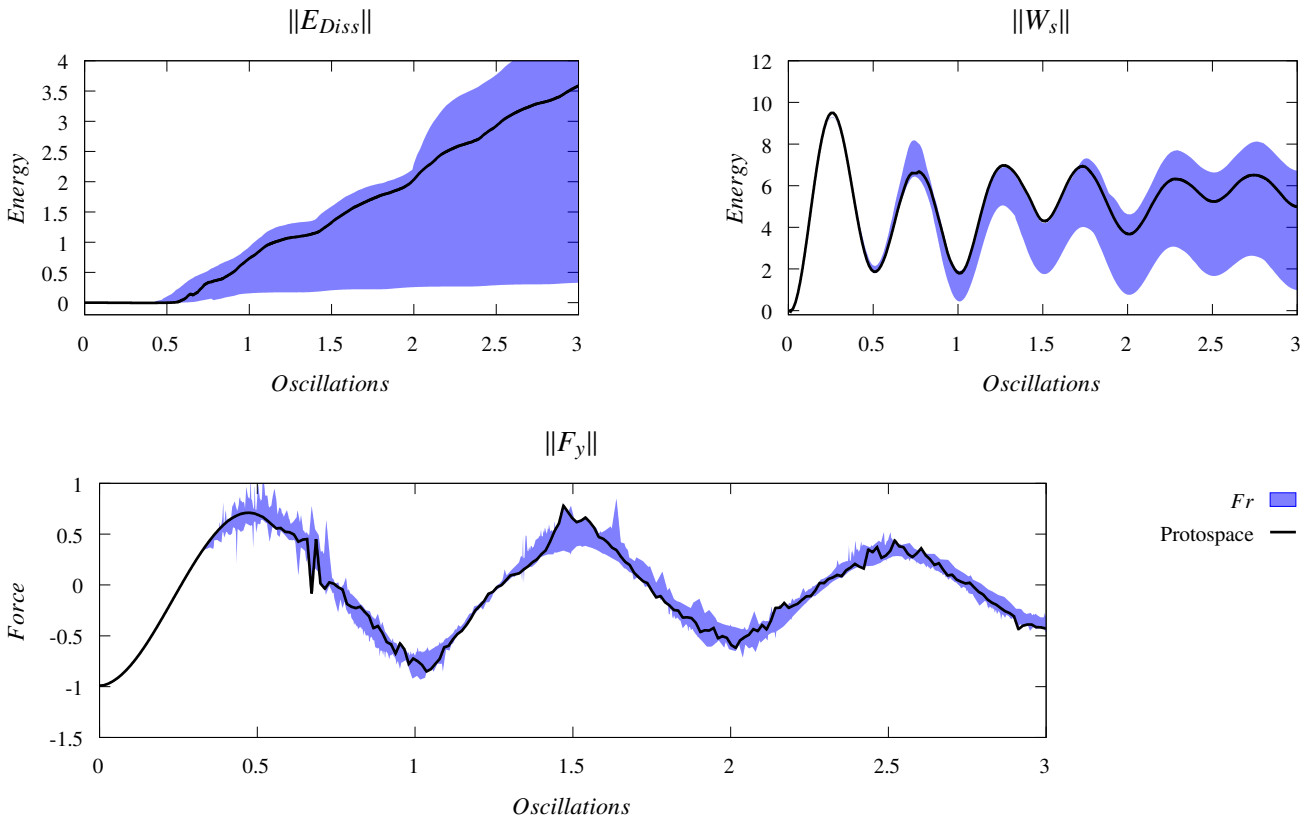

Fig. 3 Influence of Simulation Properties on Selected Normalised System Energies and Slosh Loads

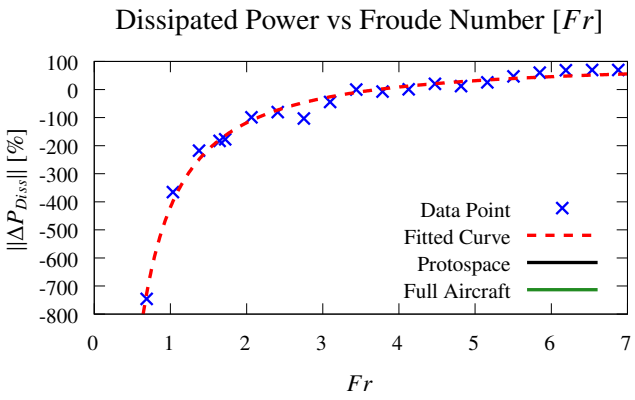

Fig. 4 Dissipated Power due to various Fluid Properties

scaling of simulation properties is evident when compared against the scaling of fluid properties.

~~Table 5 presents the analysis for the scaling of Fr. The analysis highlights the large influence for the scaling of the system excitation frequency on the fluid energies when compared to the scaling of the fluid properties. The scaling provides a large influence on RMSE value the fluid $||E_{Diss}||$ and $||W_s||$ with of $\approx$ 35% and $\approx$ 20%. The influence of the scaling on the slosh loads is similar to that of the fluid property scaling where RSME of $||F_y||$ is $\approx$ 12.5%. From Fig. 3 the scaling of the frequency ratio results in a shift in fluid impact times such that the force peaks due to fluid impact spreads between $Oscillation \approx 0.6$ and $Oscillation \approx 0.75$ as opposed to being centralised around $Oscillation \approx 0.6$.~~

Table 5 RMSE Variation due to the Simulation Property Scaling of Protospace (%)

	$\|\|E_{Diss}\|\|$	$\|\|W_s\|\|$	$\|\|F_y\|\|$
Fr	35.051	19.993	12.547

As previously done the plotting of $||\Delta P_{Disp}||$ the scaled values of the properties allows for the identification of scale-laws, within Fig. 4.

$$||\Delta P_{Diss}||(Fr) = -521.50 Fr^{-1.24} + 102.10 \quad r^2 = 0.988 \tag{15}$$

As such a scaling-law exists for the scaling of Fr with similar behaviour to the scaling of $\bar{\rho}$ as described by Eq. 15. ~~As the excitation frequency increases the dissipated power asymptotes toward $|||\Delta P_{Diss}||| = 102.10\%$ indicates decreased slosh violence at these high frequencies.~~

Scaling-laws Evaluation

To estimate the full aircraft model P_{Disp} employing ideal Froude scaling requires several fluid properties to be scaled. The fitted scaling-laws allow the prediction of the corrected Protospace for both ideal-Froude scaling (Protospace* and therefore P^*_{Disp}), employing an idealistic fluid as defined by Islam et al. (2016), and practical Froude scaling (Protospace† and similarly $P^\dagger_{Disp}$), where the full-scale model uses kerosene.

Fig. 5 presents the difference between the Protospace, ideal-Froude scaled Protospace, and true practical Froude scaled Protospace simulations. The scaling of experiments results in noticeable changes in the

Table 6 Fluid Properties and Dissipitive Power due to Froude Scaling

	Protospace	*Protospace*†	*Protospace**	*Full Aircraft*
$\bar{\rho}$	1.208×10^{-3}	1.607×10^{-3}	1.607×10^{-3}	1.607×10^{-3}
We	5.554×10^{3}	2.398×10^{3}	5.996×10^{4}	5.996×10^{4}
Re	1.616×10^{5}	4.033×10^{3}	4.509×10^{4}	4.509×10^{4}
Fr	3.440	1.648	1.648	1.648

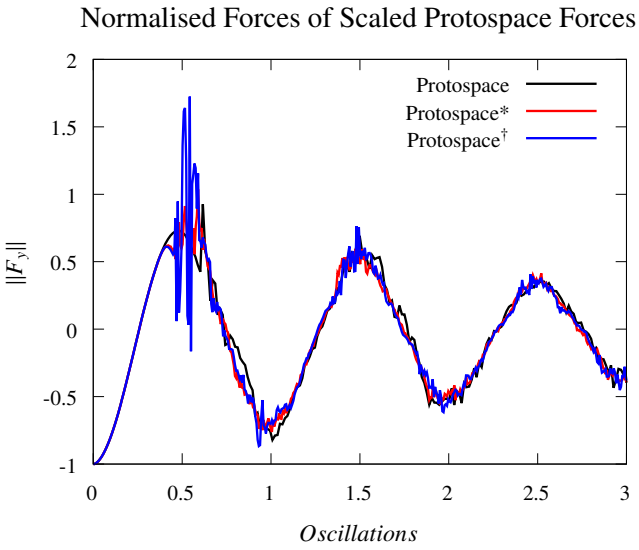

Fig. 5 Normalised Forces for Scaled Protospace Experiments

peak forces. Lighter fluid found within Protospace* and Protospace† result in earlier and high load slosh impacts. The scaling laws derived within this paper may be validated utilising comparing predicted results for P_{Disp} from the Protospace simulation against simulations for both Protospace* and Protospace‡. Where the dissipated power for the Protospace* and Protospace‡ are $P^{\ddagger}_{Disp}$(Simu) = −34.344W and P^{*}_{Disp}(Simu) = −28.211W respectively.

Employing the scaling laws derived within Fig. 2 and 4 enables to scaling of the Protosapce experiment such that:

$$P^{\ddagger}_{Disp}(\text{Calc}) = P_{Disp}\left[1 - \|\Delta P_{Disp}\|(\bar{\rho}, Fr, Re, We)\right] = -37.612W \quad (16)$$

$$P^{*}_{Disp}(\text{Calc}) = P_{Disp}\left[1 - \|\Delta P_{Disp}\|(\bar{\rho}, Fr, Re, We)\right] = -37.537W \quad (17)$$

The scaling performed in Eq. 16 and 17 employs the scaling laws defined within this study. These scaling laws provide an accuracy of 8.69% and 24.85% respectively for the calculation of $P^{\ddagger}_{Disp}$ and P^{*}_{Disp}. The accuracy in scaling found for $P^{\ddagger}_{Disp}$ occurs due to the low change in We numbers for the system. The inability to determine clear trends for the scaling of We numbers prevents the scaling laws from accounting for a factor 46 change in We between the Protospace and Protospace* simulations.

From the selected examples the scaling laws derived within this paper provides a reasonable means to estimate the power dissipation of a scaled system for the selected geometry and fill due to the scaling of $\bar{\rho}$, Fr and Re.

CONCLUSION

The proposed non-dimensional analysis of a violent sloshing FSI system has enabled the identification of functional relationship defining the slosh-damping as a function of slosh flow, fluid-structure interactions and geometric non-dimensional numbers and factors. The utilisation of high fidelity CFD simulations allows the investigation into the effects of identified fluid non-dimensional numbers ($\bar{\rho}$, Re, We, θ and Fr) in a manner would otherwise be impossible to complete through experimental campaigns.

The use of high-fidelity ELEMENTAL® CFD simulations enables the evaluation into the effects on the fluid energies, slosh loads and dissipated power for the scaling of the selected properties within the defined parameter space due to the vertical excitation of a single compartment tank experiencing damped sinusoidal acceleration. It is of interest that the scaling of Fr provides the maximum influence to the slosh loads, fluid energies and dissipated power. The fluid properties most affecting the slosh loads and dissipated power are the fluid viscosity (Re) and surface tension properties (We & θ).

The analysis enables identification of scaling laws for the scaling of $\bar{\rho}$ and Fr within the defined parameter space and the selected single compartment tank design. The evaluation of the defined scaling laws proves accurate for a selected test-case of the scaling the SLOWD Protospace experiment to provide accuracy of ≈ 9% with minimal changes in the We. This success prompts the need for future investigation to provide a robust understanding of such scaling practices on fluid energies and slosh damping for future experimental campaigns.

ACKNOWLEDGEMENTS

The research leading to these results was undertaken as part of the SLOWD project, which has received funding from the European Union's Horizon 2020 research and innovation programme under grant agreement No. 815044. The statements made herein do not necessarily have the consent or agreement of the SLOWD consortium and represent the opinion and findings of the author(s).

This work is based on research supported by the National Research Foundation of South Africa (Grant Numbers: 89916). The opinions, findings and conclusions or recommendations expressed are that of the authors alone, and the NRF accepts no liability whatsoever in this regard.

Computations were performed using facilities provided by the University of Cape Town's ICTS High Performance Computing team: hpc.uct.ac.za

REFERENCES

Gambioli, F., Chamos, A., Jones, S., Guthrie, P., Webb, J., Levenhagen, J., Behruzi, P., Mastroddi, F., Malan, A. G., Longshaw, S., Skillen, A., Cooper, J. E., González, L. & Marrone, S. (2020), Sloshing Wing Dynamics -Project Overview Sloshing Wing Dynamics – Project Overview, *in* 'Transport Research Arena 2020', number April, Helsinki, Finland.

Gambioli, F., Usach, R. A., Kirby, J., Wilson, T., Behruzi, P. & Dynamics, S. (2019), Experimental Evaluation of Fuel Sloshing Effects on Wing Dynamics, *in* 'International Forum of Aeroelasticity and Structural Dynamics (IFASD)', number June, Savannah, Georgia, USA, pp. 1–14.

Gibbings, J. C. (2011), *Dimensional Analysis*, illustrate edn, Springer Science & Business Media, Liverpool.

Heyns, J. A., Malan, A. G., Harms, T. M. & Oxtoby, O. F. (2013*a*), 'A weakly compressible free-surface flow solver for liquid-gas systems using the volume-of-fluid approach', *Journal of Computational Physics* **240**, 145–157.

Heyns, J. A., Malan, A. G., Harms, T. M. & Oxtoby, O. F. (2013*b*), 'Development of a compressive surface capturing formulation for modelling free-surface flow by using the volume-of-fluid approach', *International Journal for Numerical Methods in Fluids* **71**(6), 788–804.

Ilangakoon, N. A., Malan, A. G. & Jones, B. W. (2020), 'A higher-order accurate surface tension modelling volume-of-fluid scheme for 2D curvilinear meshes', *Journal of Computational Physics* **420**.

Islam, M., Jahra, F. & Hiscock, S. (2016), 'Data analysis methodologies for hydrodynamic experiments in waves', *Journal of Naval Architecture and Marine Engineering* **13**(1), 1–15.

Jones, B. W., Malan, A. G. & Ilangakoon, N. A. (2019), 'The initialisation of volume fractions for unstructured grids using implicit surface definitions.', *Computers and Fluids* **179**, 194–205.

Konopka, M., De Rose, F., Strauch, H., Jetzschmann, C., Darkow, N. & Gerstmann, J. (2019), 'Active slosh control and damping - Simulation and experiment', *Acta Astronautica* **158**, 89–102.

Malan, A. G. & Oxtoby, O. F. (2013), 'An accelerated, fully-coupled, parallel 3D hybrid finite-volume fluid-structure interaction scheme', *Computer Methods in Applied Mechanics and Engineering* **253**, 426–438.

Oxtoby, O. F., Malan, A. G. & Heyns, J. A. (2015), 'A computationally efficient 3D finite-volume scheme for violent liquid-gas sloshing', *International Journal for Numerical Methods in Fluids* **79**(6), 306–321.

Pattinson, J., Malan, A. G. & Meyer, J. P. (2007), 'A cut-cell non-conforming Cartesian mesh method for compressible and incompressible flow', *International Journal for Numerical Methods in Engineering* **72**(11), 1332–1354.

Summer, I. E. (1963), 'Preliminary Experimental Investigation of Frequencies and Forces Resulting from Liquid Sloshing in Toroidal Tanks', *Nasa Tn-D-1709* .

Tait, M. J. (2008), 'Modelling and preliminary design of a structure-TLD system', *Engineering Structures* **30**(10), 2644–2655.

Thompson, J. F. & Nein, M. E. (1966), 'Prediction of propellant tank pressurization requirements by dimensional analysis', *Nasa Tn-D-3451* .

Titurus, B., Cooper, J. E., Saltari, F., Mastroddi, F. & Gambioli, F. (2019), Analysis of a Sloshing Beam Experiment, *in* 'International Forum of Aeroelasticity and Structural Dynamics (IFASD)', number June, Savannah, Georgia, USA, pp. 1–18.

van Biezen, M. (2014), 'Physics - Simple Harmonic Motion with Damping (13 of 13) Energy Loss'.
URL: *https://www.youtube.com/watch?v=jvvuEIR1z80&feature=youtu.be*

Yu, J. K., Wakahara, T. & Reed, D. A. (1999), 'A non-linear numerical model of the tuned liquid damper', *Earthquake Engineering and Structural Dynamics* **28**(6), 671–686.